Real-Time Control of Electronic Motion: Application to HD^+

Michael Grønager and Niels E. Henriksen*

Department of Chemistry, Technical University of Denmark, DTU 207, DK 2800 Lyngby, Denmark

Received: October 1, 1997; In Final Form: December 1, 1997

We show that a nonstationary electron can be created in HD^+ corresponding to partial electron transfer between H^+ and D^+. The electronic motion is introduced through nuclear motion, more specifically, through nonadiabatic curve crossing, and the electronic motion is here on the same time scale as the nuclear motion. We show that the branching ratio between the channels $H + D^+$ and $H^+ + D$ depends on the electron distribution (i.e., where the electron "sits") prior to the time where the bond is broken by an infrared femtosecond pulse. Thus, we control—in real-time—which nucleus the electron will follow after the bond is broken.

I. Introduction

The real-time monitoring and control of chemical dynamics is at the heart of femtochemistry.[1−3] To that end, a challenging objective is to control bond breaking in polyatomic molecules and to control electron transfer during bond breaking, that is, to control which nuclei the (valence) electrons will follow when a specific bond is broken.

In a previous letter[4] we have discussed an explicitly time-dependent double-pulse laser control scheme for controlling where nuclei and electrons are going in unimolecular reactions. The basic principle used is in the spirit of the scheme of Tannor and Rice,[5,6] that is, vibrational or electronic wave packets are created and controlled by time-delayed ultrashort laser pulses. In this paper we focus on electronic motion and test the scheme on the HD^+ molecule. The real-time control of electronic motion has been suggested before for atoms, Krause et al. has, for example, considered wave packet motion of Rydberg states in the hydrogen atom.[7] The electronic motion of H_2^+ in intense laser fields has also been studied.[8]

The first step in the scheme is to create a nonstationary electron corresponding to (partial) electron transfer between different atoms in a molecule.[4,9] The electronic motion is introduced via nuclear motion, more specifically, when a vibrational wave packet moves through a nonadiabatic curve crossing. In an adiabatic representation, the molecular wave function has components in more than one electronic state when the wave packet moves through the crossing region and the electron is, accordingly, nonstationary. In addition, the electronic motion is here on the same time scale as the nuclear motion. The second step in the scheme is to break the chemical bond between the atoms at an appropriate time. Thus, depending on the electron distribution prior to the time where the bond is broken by a femtosecond pulse, we can (at least, partially) control electron transfer between the separated atoms.

In this paper, we want to demonstrate the principle behind real-time control of electronic motion in a molecule. The calculations we present here are based on simple (Gaussian) pulses with an appropriate time delay, that is, no optimized pulses are invoked (see refs 7, 10−13 and references therein).

HD^+ is a simple molecule that has been studied extensively, experimentally as well as theoretically.[14−19] The electronic states as well as the non-adiabatic couplings can be found semianalytically,[15−19] and hence the properties of the nonrelativistic molecule can be found with an arbitrary precision. It is, accordingly, a simple system where the calculations leave little or no room for speculations concerning the validity of approximations. These facts makes HD^+ a good test system for the control scheme described above.[4]

When applied to HD^+ the scheme consists of (1) the preparation of an oscillating electron associated with a highly excited vibrational state in the molecule (denoted by $(HD^+)^*$), and (2) the dissociation of this nonstationary state. Thus,

$$(HD^+)^* \xrightarrow{h\nu} \begin{cases} H + D^+ \\ H^+ + D \end{cases} \tag{1}$$

and the time of the dissociation is expected to have a controlling influence on the branching ratio. That is, the aim is to catch and freeze the oscillating electron distribution by the laser pulse that breaks the bond.

Electronic control in HD^+ has been studied previously in a time-independent framework. Sheehy et al.[20] and Ghosh et al.[21,22] has shown the possibility of control when the relative intensity of two intense laser fields is varied. Charron et al.[23] has used an intense field two-color coherent control scheme[24−27] to dissociate HD^+ showing a very high degree of controllability.

The present work should be considered as a demonstration of a principle for real-time electronic control. The control scheme we apply to HD^+ might not offer the same high degree of controllability as the ones above, neither we shall claim that this scheme is simpler to implement. The control scheme used here might, however, be better suited for other molecules. The implementation on NaI is in progress.[28]

The paper is organized as follows. In section II we derive equations of motion directly from the three particle nonrelativistic Schrödinger equation. We separate coordinates in center of mass, electronic, and nuclear coordinates taking into account the different mass of the proton and deuteron. We separate out the rotation and is left with a one-dimensional vector equation for the motion of the nuclei. In section III we find vibrational eigenstates, and examine a highly excited vibrational state showing a oscillating electron distribution. Finally, we show that the use of an infrared femtosecond pulse fired at the right time has a controlling influence on the branching ratio. To that end we vary the pulse width and frequency in order to optimize the yield and the controllability.

S1089-5639(97)03198-8 CCC: $15.00
Published on Web 02/03/1998

II. Theory

There are two different choices of the internal coordinates once the separation from laboratory coordinates to center of mass coordinates is done. One can use either Jacobi coordinates where the position of the electron is measured relative to the center of mass of the nuclei (see, for example, ref 15) or Geometric coordinates where the position of the electron is measured relative to the geometrical center of the nuclei (see, for example, ref 18). The choice of the latter introduces a mass polarization term whereas the Jacobi coordinates hides the mass polarization in the potentials and the in the nonadiabatic coupling. It should be noted that the two coordinate systems coincide if the nuclei are identical, for example, for H_2^+. Further it should be noted that the choice of coordinate system, of course, by no means influence the results. We shall in this paper use the Jacobi coordinates.

A. Separation of Coordinates. The separation of coordinates goes as follows; first we separate out the center of mass motion, second, focusing on the molecule in the center of mass frame, we separate the electronic and nuclei motion, and finally we separate the angular variables. We shall essentially follow the general three-body derivation by Hunter et al.[15] However, we shall introduce a laser field in the Hamiltonian and further we shall introduce some simplifications possible only for the HD^+-system. Where our derivation is similar to the derivation of Hunter et al., we shall indeed be short and only highlight the conceptually important results.

The total nonrelativistic Hamiltonian in laboratory coordinates within the electric dipole approximation writes:

$$\hat{H}_{\text{tot}} = -\frac{\hbar^2}{2m_{\text{p}}}\nabla_{\text{p}}^2 - \frac{\hbar^2}{2m_{\text{d}}}\nabla_{\text{d}}^2 - \frac{\hbar^2}{2m_{\text{e}}}\nabla_{\text{e}}^2 + V(r_{\text{pd}}, r_{\text{pe}}, r_{\text{de}}) - e\mathbf{E}(t)\cdot(\mathbf{x}_{\text{p}} + \mathbf{x}_{\text{d}} - \mathbf{x}_{\text{e}}) \quad (2)$$

where m denotes mass, x denotes position and r denotes interparticle distance. Subindices p, d, and e denotes proton, deuteron, and electron respectively. V is the usual Coulomb potential of the interparticle distances and $\mathbf{E}(t)$ is the electric field. By transforming to Jacobi coordinates, we can separate out the center of mass motion:

$$\begin{bmatrix}\mathbf{X}\\ \mathbf{x}\\ \mathbf{X}\end{bmatrix} = \begin{bmatrix}-1 & 1 & 0\\ -\frac{m_{\text{p}}}{m_{\text{p}}+m_{\text{d}}} & -\frac{m_{\text{d}}}{m_{\text{p}}+m_{\text{d}}} & 1\\ \frac{m_{\text{p}}}{M} & \frac{m_{\text{d}}}{M} & \frac{m_{\text{e}}}{M}\end{bmatrix}\begin{bmatrix}\mathbf{x}_{\text{p}}\\ \mathbf{x}_{\text{d}}\\ \mathbf{x}_{\text{e}}\end{bmatrix} \quad (3)$$

where $M = m_{\text{p}} + m_{\text{d}} + m_{\text{e}}$. We can hence write the total Hamiltonian as the sum of a center of mass Hamiltonian:

$$\hat{H}_{\text{cm}} = -\frac{\hbar^2}{2M}\nabla_{\mathbf{X}}^2 - e\mathbf{E}(t)\cdot\mathbf{X} \quad (4)$$

and a molecular Hamiltonian:

$$\hat{H}_{\text{mol}} = -\frac{\hbar^2}{2M}\nabla_{\mathbf{X}}^2 - \frac{\hbar^2}{2m}\nabla_{\mathbf{x}}^2 + V(\mathbf{X}, \mathbf{x}) - e\mathbf{E}(t)\cdot\left[\left(\frac{m}{m_{\text{e}}} - 2\right)\mathbf{x} + \frac{m_{\text{p}} - m_{\text{d}}}{m_{\text{d}} + m_{\text{p}}}\mathbf{X}\right] \quad (5)$$

with $M^{-1} = m_{\text{p}}^{-1} + m_{\text{d}}^{-1}$ and $m^{-1} = (m_{\text{p}} + m_{\text{d}})^{-1} + m_{\text{e}}^{-1}$. We can hence write the total wave function as a product wave function:

$$\psi_{\text{tot}}(\mathbf{X}, \mathbf{x}, \mathbf{X}) = \psi_{\text{cm}}(\mathbf{X})\psi_{\text{mol}}(\mathbf{X}, \mathbf{x}) \quad (6)$$

We now introduce the Born−Huang expansion[29] for the molecular wave function:

$$\psi_{\text{mol}}(\mathbf{X}, \mathbf{x}) = \zeta^{3/2}\sum_j \varphi_j(\zeta\mathbf{x}, \zeta\mathbf{X})\chi_j(\mathbf{X}) \quad (7)$$

With $\zeta = m_{\text{e}}m_{\text{d}}/m(m_{\text{e}} + m_{\text{d}})$ (see ref 15). The *electronic* wave functions φ_j are chosen as solutions to the *electronic* Schrödinger equation

$$\hat{H}_{\text{elec}}\varphi_j(\mathbf{x}, \mathbf{X}) = W_j(R)\varphi_j(\mathbf{x}, \mathbf{X}) \quad (8)$$

where $R = |\mathbf{X}|$, and where $\hat{H}_{\text{elec}}$ is the *electronic* Hamiltonian

$$\hat{H}_{\text{elec}} = -\frac{\hbar^2}{2m}\nabla_{\text{x}}^2 + V(\mathbf{X}, \mathbf{x}) \quad (9)$$

In order to solve this equation we first transform $\mathbf{x}$ to a coordinate system rotating with the nuclei (i.e., with $\mathbf{X}$). We define the spherical polar coordinates of $\mathbf{X}$ as (R,ϕ,θ) and rotate and displace $\mathbf{x}$ according to the following transformation:

$$\begin{bmatrix}x'\\ y'\\ z'\end{bmatrix} = \begin{bmatrix}0\\ 0\\ \alpha R\end{bmatrix} + \begin{bmatrix}-\cos(\phi)\cos(\theta) & -\sin(\phi)\cos(\theta) & \sin(\theta)\\ \sin(\phi) & -\cos(\phi) & 0\\ \cos(\phi)\sin(\theta) & \sin(\phi)\sin(\theta) & \cos(\theta)\end{bmatrix}\begin{bmatrix}x\\ y\\ z\end{bmatrix} \quad (10)$$

where (x, y, z) and $(x' y', z')$ are the Cartesian coordinates of $\mathbf{x}$ and $\mathbf{x}'$, respectively, and where $\alpha = (m_{\text{d}} - m_{\text{p}})/(2(m_{\text{d}} + m_{\text{p}})) \simeq {}^1/_6$. Now $\mathbf{x}'$ is centered in the geometrical center of the nuclei and is rotating with the bond axis.

We now introduce prolate spheroidal coordinates (u, v, ω) for $\mathbf{x}'$ by ref 30:

$$x' = {}^1/_2 R\cos\omega\sqrt{(u^2-1)(1-v^2)} \quad (11a)$$

$$y' = {}^1/_2 R\sin\omega\sqrt{(u^2-1)(1-v^2)} \quad (11b)$$

$$z' = {}^1/_2 Ruv \quad (11c)$$

These coordinates separate the electronic Schrödinger equation, ref 31:

$$\frac{\partial}{\partial u}(u^2-1)\frac{\partial \Upsilon}{\partial u} + \left(-C - p^2(u^2-1) - \frac{\mu^2}{u^2-1} + \frac{2me^2}{4\pi\epsilon_0\hbar^2}Ru\right)\Upsilon = 0 \quad (12a)$$

$$\frac{\partial}{\partial v}(1-v^2)\frac{\partial \Xi}{\partial v} + \left(C - p^2(1-v^2) - \frac{\mu^2}{1-v^2}\right)\Xi = 0 \quad (12b)$$

$$\frac{\partial^2 \Omega}{\partial \omega^2} + \mu^2\Omega = 0 \quad (12c)$$

Where $\varphi_j = \Upsilon_{\nu\mu\lambda}(u)\Xi_{\nu\mu\lambda}(v)\Omega_\mu(\omega)$ and where $p = R\sqrt{-{}^1/_2 mW_j}$, and where C is the separation constant of the two coupled Sturm−Liouville equations, eqs 12a,b. The ω-equation is easily solved to give $\Omega(\omega) = {}^1/_{2\pi}e^{\pm i\mu\omega}$. Equations 12a,b are

solved by introducing the infinite series expansions:

$$\mathrm{Y}_{\nu\mu\lambda}(u, R) = \mathrm{e}^{-p(u-1)}(p(u-1))^{\lambda}\sum_{n=1}^{\infty} a_n^{\nu\mu\lambda}(R) L_{n-\lambda-1}^{2\lambda+1}(2p(u-1)) \tag{13a}$$

$$\Xi_{\nu\mu\lambda}(v, R) = \sum_{l=0}^{\infty} b_l^{\nu\mu\lambda}(R) P_l^{\mu}(v) \tag{13b}$$

where L and P are associated Laguerre and Legendre polynomials, respectively, ref 30. Inserting eqs 13a,b in eqs 12a,b yields recurrence relations for a_n and b_l.[32] Equations 12a,b are now solved simultaneously, using 2D-Newton−Raphson iteration for (C, p).[32,33] We start the calculation at small internuclear separations using the united atom results, $R \sim 0$; $C \sim \lambda(\lambda+1)$ and $W \sim 2^2/2mv^2$ as first guesses. (C, p) for $R > 0$ is obtained using the results at smaller R as first guesses.

We shall only be concerned with the two lowest electronic states, $1s\sigma_g$ and $2p\sigma_u$. The second excited state and up is at all internuclear distances of much higher energy than $1s\sigma_g$ and $2p\sigma_u$ and can hence safely be neglected.

The $1s\sigma_g$ and $2s\sigma_u$ correspond to (ν, μ, λ) equal to (1,0,0) and (2,0,1), respectively. I.e., we have that the angular momentum of the electron $\mu = 0$ and hence the total angular momentum is equal to the angular momentum of the nuclei.

B. Nuclear Schrödinger Equation. We shall now consider the nuclear Schrödinger equation. We insert the Born−Huang expansion for the molecular wave function, eq 7, into the molecular Schrödinger equation, multiply by $\zeta^{3/2}\varphi_i(\zeta\mathbf{x}, \zeta\mathbf{X})\chi_i(\mathbf{X})$ and integrate over electronic coordinates. We obtain

$$i\hbar\frac{\mathrm{d}}{\mathrm{d}t}\begin{bmatrix}\chi_1(R,\theta,\phi)\\ \chi_2(R,\theta,\phi)\end{bmatrix} = \left\{\begin{bmatrix}\hat{T}_{11}(R) & \hat{T}_{12}(R)\\ \hat{T}_{21}(R) & \hat{T}_{22}(R)\end{bmatrix} + \begin{bmatrix}V_{11}(R) & V_{12}(R)\\ V_{21}(R) & V_{22}(R)\end{bmatrix} - \mathrm{e}E(t)\begin{bmatrix}D_{11}(R) & D_{12}(R)\\ D_{21}(R) & D_{22}(R)\end{bmatrix}\cos\theta\right\}\begin{bmatrix}\chi_1(R,\theta,\phi)\\ \chi_2(R,\theta,\phi)\end{bmatrix} \tag{14}$$

where we, as stressed above, only consider the $1s\sigma_g$ and the $2p\sigma_u$ states (abbreviated to subscripts 1 and 2, respectively) and used the orthonormality of φ_j. $\hat{T}_{ij}(R)$ is the kinetic energy operator and $V_{ij}(R)$ potential energy. Since we are only considering transitions between states with the same electronic quantum number ($\mu = 0$), the off-diagonal in the potential energy matrix becomes independent of the rotation of the nuclei, governed by the variables θ and ϕ. $D_{ij}(R)$ is the electric dipole moment operator for a field in the laboratory z-direction. We see that the only angular dependence is associated with the electric dipole moment, and hence when the field $E(t)$ is off, the dimensionality of the problem reduces considerably.

The electronic dipole moment operator can be written as

$$D_{ij}(R) = -\left[\alpha\left(1 - \frac{m_e}{M}\right)\delta_{ij} + \frac{1}{2}\left(1 + \frac{m_e}{M}\right)\mathrm{DM}_{ij}(R)\right]R \tag{15}$$

with

$$\mathrm{DM}_{ij}(R) = \frac{\zeta^3 R^3}{8}\int_0^{2\pi}\int_{-1}^{1}\int_{1}^{\infty}\varphi_i(u, v, \omega, \zeta R)\times \varphi_j(u, v, \omega, \zeta R)uv(u^2 - v^2)\mathrm{d}u\mathrm{d}v\mathrm{d}\omega \tag{16}$$

For large internuclear separations one can obtain simple expressions for the electric dipole moments. These are found by inserting the asymptotic solutions for the electronic wavefunctions, namely 1s orbitals on the proton and the deuteron. We find that $\mathrm{DM}_{12} = \mathrm{DM}_{21} \rightarrow 1$ and obtain:

$$D_{11}/R = D_{22}/R = -\alpha(1 - m_e/M) \simeq -{}^1/_6 \tag{17a}$$

$$D_{12}/R = D_{21}/R = -{}^1/_2(1 + m_e/M) \simeq -{}^1/_2 \tag{17b}$$

for $R \rightarrow \infty$. However, this limit is valid as a good approximation in the range from $\sim 2\ b$ to infinity.

An expression for the sum $\hat{T}_{ij} + V_{ij}$ can be found in the extensive paper of Hunter, Gray, and Pritchard.[15] However, an error herein should be corrected; eq 30 should read (in the notation of Hunter et al.):

$$H(R)_{ij} = -\frac{1}{4}Q(R)_{ij} + \frac{(m^2-3)\delta_{ij}}{4R^2} - \frac{1}{64}R^3[E_e(R)_i + E_e(R)_j]\int K_iK_j(\lambda^4 - \mu^4)\mathrm{d}\mu\mathrm{d}\lambda - \frac{1}{8}R^2\int K_iK_j(\lambda^2+\mu^2)[\lambda(q+1) + \mu(q-1)]\mathrm{d}\mu\mathrm{d}\lambda - \frac{1}{8}R^3\int\frac{\partial K_i}{\partial R}\frac{\partial K_j}{\partial R}(\lambda^2-\mu^2)\mathrm{d}\mu\mathrm{d}\lambda - \frac{1}{8}R^2\int\left[\lambda(1-\lambda^2)\left(\frac{\partial K_i}{\partial\lambda}\frac{\partial K_j}{\partial R} + \frac{\partial K_j}{\partial\lambda}\frac{\partial K_i}{\partial R}\right) + \mu(\mu^2-1)\left(\frac{\partial K_i}{\partial\mu}\frac{\partial K_j}{\partial R} + \frac{\partial K_j}{\partial\mu}\frac{\partial K_i}{\partial R}\right)\right]\mathrm{d}\mu\mathrm{d}\lambda \tag{18}$$

Now for the nuclear wave function, $\chi_i(R, \theta, \phi)$, we insert in the nuclear Schrödinger equation, eq 14, the sum of products:

$$\chi_j(R, \theta, \phi) = \frac{1}{R}\sum_{l=0}^{\infty}\sum_{m=-l}^{l} Y_{lm}(\theta, \phi)\chi_{jlm}(R) \tag{19}$$

where $Y_{lm}(\theta, \phi)$ are spherical harmonics. We multiply with $Y_{l'm'}(\theta, \phi)$ and integrate over θ and ϕ and finally multiply by R. We hence get the equation:

$$i\hbar\frac{\mathrm{d}}{\mathrm{d}t}\begin{bmatrix}\chi_{1lm}(R)\\ \chi_{2lm}(R)\end{bmatrix} = \sum_{l=0}^{\infty}\left\{-\frac{\hbar^2}{2M}\delta_{ll'}\begin{bmatrix}\frac{\mathrm{d}^2}{\mathrm{d}R^2} - g^2 - \frac{l(l+1)}{R^2} & -2g\frac{\mathrm{d}}{\mathrm{d}R} + \frac{\mathrm{d}g}{\mathrm{d}R}\\ 2g\frac{\mathrm{d}}{\mathrm{d}R} - \frac{\mathrm{d}g}{\mathrm{d}R} & \frac{\mathrm{d}^2}{\mathrm{d}R^2} - g^2 - \frac{l(l+1)}{R^2}\end{bmatrix} + \delta_{ll'}\begin{bmatrix}V_{11}(R) & V_{12}(R)\\ V_{21}(R) & V_{22}(R)\end{bmatrix} - \mathrm{e}A_{ll'}^m E(t)\begin{bmatrix}D_{11}(R) & D_{12}(R)\\ D_{21}(R) & D_{22}(R)\end{bmatrix}\right\}\begin{bmatrix}\chi_{1l'm}(R)\\ \chi_{2l'm}(R)\end{bmatrix} \tag{20}$$

where

$$A_{ll'}^m = \int_0^{2\pi}\int_0^{\pi} Y_{lm}(\theta, \phi)\cos\theta Y_{l'm}(\theta, \phi)\sin\theta\,\mathrm{d}\theta\,\mathrm{d}\phi \tag{21}$$

is a tridiagonal matrix with $A_{l,l-1}^m = A_{l-1,l}^m = \sqrt{(l^2-m^2)/(4l^2-1)}$. $g(R)$ and $V_{ij}(R)$ can be found in ref 15.

In this paper we shall only consider the rotational ground state, $l = 0$. For a weak field we will only have one-photon transitions, and we will neglect the addition of one unit of angular momentum. Since $V_{jj}(R)$ dominates over $\hbar^2 l(l+1)/(2MR^2)$ this approximation is justified. We shall hence label the scalar states of the vibrational vector state, $\chi_1(R)$ and $\chi_2(R)$ omitting the $l = 0$ and $m = 0$ subscripts.

We now introduce two new representations: The *diabatic*/ and the *true adiabatic*/ representation. In the diabatic representation the kinetic energy matrix is diagonal and in the true adiabatic representation the potential energy matrix is diagonal. In the representation used so far neither the kinetic nor the potential energy matrices are diagonal, we label this representation the adiabatic representation, as it is the one we get diagonalizing the electronic Hamiltonian. However, due to the inclusion of the mass polarization term in the treatment (the mass of the nuclei are not taken to be infinite), we get a small off diagonal contribution to the potential energy matrix. By diagonalization of this matrix we obtain the true adiabatic representation.

A transformation between any of the representations considered can be performed by the unitary matrix:

$$\begin{bmatrix} \cos\Theta(R) & -\sin\Theta(R) \\ \sin\Theta(R) & \cos\Theta(R) \end{bmatrix} \tag{22}$$

where $\Theta(R)$ is chosen to diagonalize either the kinetic or the potential energy matrix.[34] The true adiabatic representation is unique, whereas the diabatic representation can be rotated arbitrarily with a constant Θ_∞. We shall choose the diabatic representation that is asymptotic with the two product channels namely an electron in a 1s-orbital on either the deuteron or on the proton. This corresponds to $\chi_1^{\mathrm{D}}(R) = 1/\sqrt{2}[\chi_1(R) + \chi_2(R)]$ and $\chi_2^{\mathrm{D}}(R) = 1/\sqrt{2}[\chi_1(R) - \chi_2(R)]$ where $\chi_j^{\mathrm{D}}(R)$ is the nuclear wave function in the diabatic representation. With this choice, the diabatic and true adiabatic representations coincides in the asymptotic region. Further the diabatic representation gives a direct measure of the magnitude of the electron density on the proton/deuteron, respectively.

The Schrödinger equation in the diabatic representation writes:

$$i\hbar\frac{\mathrm{d}}{\mathrm{d}t}\begin{bmatrix}\chi_1^{\mathrm{D}}(R)\\ \chi_2^{\mathrm{D}}(R)\end{bmatrix} = \left\{ -\frac{\hbar^2}{2M}\begin{bmatrix}\frac{\mathrm{d}^2}{\mathrm{d}R^2} & 0\\ 0 & \frac{\mathrm{d}^2}{\mathrm{d}R^2}\end{bmatrix} + \begin{bmatrix}V_{11}^{\mathrm{D}}(R) & V_{12}^{\mathrm{D}}(R)\\ V_{21}^{\mathrm{D}}(R) & V_{22}^{\mathrm{D}}(R)\end{bmatrix} - eE(t)\begin{bmatrix}D_{11}^{\mathrm{D}}(R) & D_{12}^{\mathrm{D}}(R)\\ D_{21}^{\mathrm{D}}(R) & D_{22}^{\mathrm{D}}(R)\end{bmatrix}\right\}\begin{bmatrix}\chi_1^{\mathrm{D}}(R)\\ \chi_2^{\mathrm{D}}(R)\end{bmatrix} \tag{23}$$

where $V_{ij}^{\mathrm{D}}(R)$ and $D_{ij}^{\mathrm{D}}(R)$ are the potential energy and the electric dipole moment transformed into the diabatic representation. We use the diabatic representation for the computation as the diagonality of the kinetic energy matrix simplifies the evaluation of the Hamiltonian considerably.[35]

The Schrödinger equation in the true adiabatic representation is similar to eq 20 except that the potential energy matrix is diagonal. In Figure 1, we have plotted the diagonal of the potential energy matrix which we label $\mathbf{V}_{11}^{\mathrm{T}}(R)$ and $\mathbf{V}_{22}^{\mathrm{T}}(R)$; and furthermore, we have plotted $(g^{\mathrm{T}}(R))^2/2M$, again the superscript "T" denotes the true adiabatic representation. We see that the coupling term peaks around the avoided crossing at 11.8 *b* and that $\mathbf{V}_{22}^{\mathrm{T}}(R)$ supports an adiabatic well, a very shallow one that is.

We shall now examine the electric dipole moments in order to clarify whether or not it is possible to freeze the electronic motion in the breaking of the bond. That is, we do not want the electron to move due to the influence of the field. To that end, we consider the system in the diabatic representation; here the two states gives a direct measure of how much of the electron that is on the proton vs. the deuteron. An approximation for the electric dipole moments in the diabatic representation can be calculated from eqs 17a,b and eq 22. We obtain:

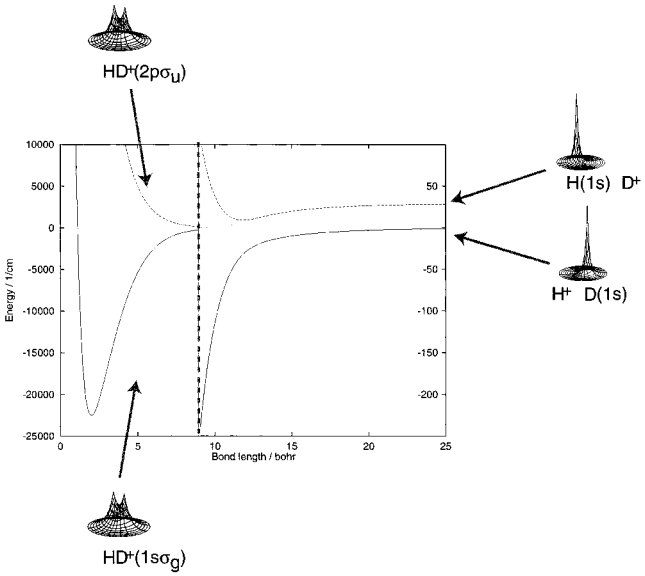

Figure 1. The true adiabatic potentials (solid and dashed) and the coupling (dotted) for HD^+ (see text). Near the equilibrium bond distance, the electron is equally shared between the nuclei and the true adiabatic and the adiabatic potential are almost identical. In the plot we have indicated this labeling of the potentials according to the adiabatic states. In the asymptotic region (magnified by a factor of 100), the true adiabatic potential resembles the two dissociation channels and is hence labeled accordingly. Note that the adiabatic well is very shallow and note further the small splitting between the two dissociation channels $H^+ + D$ and $H + D^+$.

$$D_{12}^{\mathrm{D}}/R = D_{21}^{\mathrm{D}}/R \sim 0 \tag{24a}$$

$$D_{11}^{\mathrm{D}}/R \sim (\alpha - {}^1/_2) - \frac{m_{\mathrm{e}}}{M}(\alpha + {}^1/_2) \simeq {}^1/_3 \tag{24b}$$

$$D_{22}^{\mathrm{D}}/R \sim (\alpha + {}^1/_2) - \frac{m_{\mathrm{e}}}{M}(\alpha - {}^1/_2) \simeq -{}^2/_3 \tag{24c}$$

These dipole moments are valid in the range from ~ 2 *b* to infinity. We see that a (diabatic) electronic transition governed by D_{12}^{D} is very unlikely; furthermore, we see that (diabatic) vibrational transitions can occur, of course, depending on the vibrational Franck−Condon factors. It should be noted that the probabilities associated with laser excitation into the translational continuum states of the two channels, in general, are different. Thus, the dipole moments differ by a factor of 2, and in addition, the vibrational Franck−Condon factors can be different (depending on the laser frequency). These findings suggests, nevertheless, that we should be able to freeze the electronic motion in the breaking of the bond, and hence control the branching ratio. That is, the magnitude of the electron density on the proton vs deuteron before and after the bond is broken can be unchanged (when the laser parameters are properly chosen).

It should be stressed, that in the calculations done in the following section, we use the exact dipole moments, and not the above approximation.

III. Results and Discussion

In this section we shall examine the highly excited vibrational eigenstates of HD^+ to clarify the asymmetric behaviour due to the different mass of the proton and the deuteron. Further we shall examine the possibility of controlling the dissociation into either $H^+ + D$ or $H + D^+$.

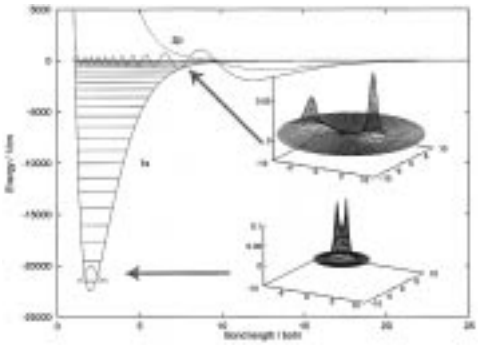

Figure 2. Adiabatic representation of all vibrational eigenlevels, the vibrational ground state, and the 21st vibrational excited state. The potential for the electronic ground state and the absolute square of the corresponding part of the vibrational eigenstates are in solid and the potential for the electronic excited state and the absolute square of the corresponding part of the vibrational eigenstates are dashed. Also shown is the electron density for the two specific states.

A. Vibrational Eigenstates. For $l = 0$, HD^+ has 23 bound vibrational eigenstates (see, for example, ref 18); the 22nd vibrational excited state, however, is bound with only a few cm^{-1}. We shall hence only consider the first 22 states.

We solve the time-independent Schrödinger equation in the diabatic representation:

$$\left\{-\frac{\hbar^2}{2M}\begin{bmatrix}\frac{d^2}{dR^2} & 0\\ 0 & \frac{d^2}{dR^2}\end{bmatrix}+\begin{bmatrix}V_{11}^{D}(R) & V_{12}^{D}(R)\\ V_{21}^{D}(R) & V_{22}^{D}(R)\end{bmatrix}\right\}\begin{bmatrix}\chi_{1,n}^{D}(R)\\ \chi_{2,n}^{D}(R)\end{bmatrix}=\epsilon_n\begin{bmatrix}\chi_{1,n}^{D}(R)\\ \chi_{2,n}^{D}(R)\end{bmatrix} \quad (25)$$

where ϵ_n is the energy eigenvalue of the n'th vibrational vector eigenstate, $\chi_{j,n}^{D}(R)$. However, instead of solving eq 25 directly, we propagate eq 23 with $E(t) = 0$ in imaginary time.[36] The computation is performed on two 512 point grids (one for each scalar state in the vibrational vector state) with a position spacing of 0.1 b. By using the Chebychev propagator[37,38] (as compared to the split propagator[39,40]) we avoid the transform (forward and back) between the adiabatic and the diabatic representation in each time step.[35]

In Figure 2, we have plotted the adiabatic potentials, all vibrational eigenvalues, the vibrational ground state, and the 21st vibrational excited state. The adiabatic potential for the electronic ground state and the absolute square of the respective part of the vibrational eigenstates are in solid, whereas the adiabatic potential for the excited electronic state and the absolute square of the respective part of the vibrational eigenstates are dashed. We see that the 21st vibrational excited state has a considerable contribution on both electronic states and is hence asymmetric. (I.e., it is more likely to find the electron on the deuteron than on the proton). This is more evident from the electron density which is also plotted in Figure 2. The electron density can be found directly from the vibrational eigenstates in the adiabatic representation, simply by integrating out the nuclear coordinates, after transforming from the diabatic to the adiabatic representation:

$$P(u, v) = \sum_{i,j=1,2}\int_0^\infty \varphi_i(u, v, R)\chi_i^*(R)\varphi_j(u, v, R)\chi_j(R)\,dR = \int_0^\infty[\varphi_1\chi_1^*\varphi_1\chi_1 + \varphi_2\chi_2^*\varphi_2\chi_2 + 2\mathrm{Re}(\varphi_1\chi_1^*\varphi_2\chi_2)]\,dR \quad (26)$$

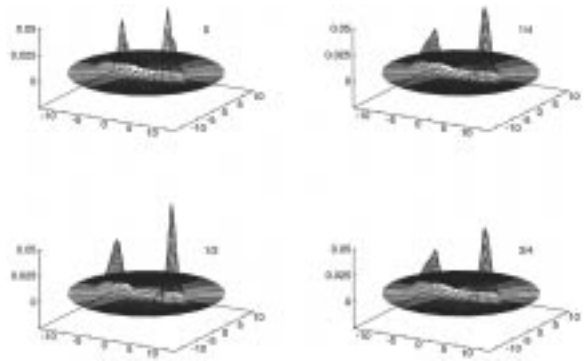

Figure 3. The oscillating electron density at times 0, $^1/_4$, $^1/_2$, and $^3/_4$ of the vibration period. The electron density is defined in eq 26.

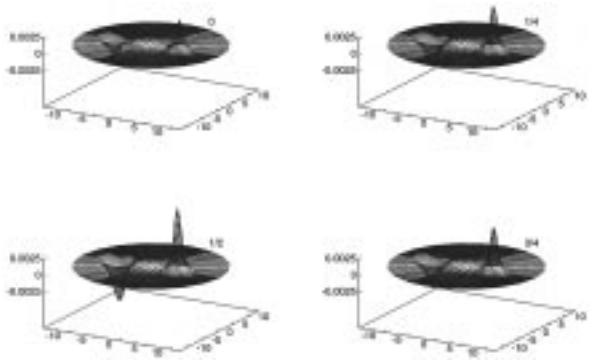

Figure 4. Electron difference plot at times 0, $^1/_4$, $^1/_2$, and $^3/_4$ of the vibration period. The electron difference shows the electron transfer as defined in the text.

We have here suppressed the coordinate dependence for the electronic and nuclear wave functions. In the following we shall do likewise where it is unambiguous.

B. Oscillating Electron. We now make a coherent superposition of the 20st and the 21st vibrationally excited eigenstate. Since they both show an asymmetric electronic density, we would expect that in this superposition the electron would oscillate between the proton and the deuteron. However, the electron oscillates in such a way that the probability that the electron is near the proton never exceeds 50%. The preparation of this state could, for example, be accomplished using a series of infrared picosecond laser pulses, similar to the preparation of highly excited vibrational eigenstates by Korolkov et al.[41]

At $t = 0$ the system is prepared in the coherent superposition:

$$\begin{bmatrix}\chi_1^{D}(t=0)\\ \chi_2^{D}(t=0)\end{bmatrix}=\frac{\sqrt{2}}{2}\left\{\begin{bmatrix}\chi_{1,20}^{D}\\ \chi_{2,20}^{D}\end{bmatrix}+\begin{bmatrix}\chi_{1,21}^{D}\\ \chi_{2,21}^{D}\end{bmatrix}\right\} \quad (27)$$

We now follow the dynamics of this state for an entire vibration period $\tau = 2\pi\hbar/(\epsilon_{21} - \epsilon_{20}) = 393$ fs. We display the motion as four snapshots at times $t = 0$, $\tau/4$, $\tau/2$, and $3\tau/4$. Figure 3 shows the electron density as defined in eq 26, and Figure 4 shows an *electron difference plot*, defined as the last term of the integral in eq 26, $\int_0^\infty \mathrm{Re}[\varphi_1\chi_1^*\varphi_2\chi_2]\,dR$ which is responsible for any asymmetric effect in the electron density. Figure 5 shows the expectation value of the internuclear separation R and the percentage of the electron density near the proton vs. the deuteron calculated as the percentage of probability on the diabatic surfaces. From these figures, it is clear that the electron and the nuclei move on the same time scale. (I.e., as the molecule vibrates, the electron moves from the proton to the deuteron and back). This is a clear breakdown of the adiabatic approximation and suggests that, if we could break the bond at

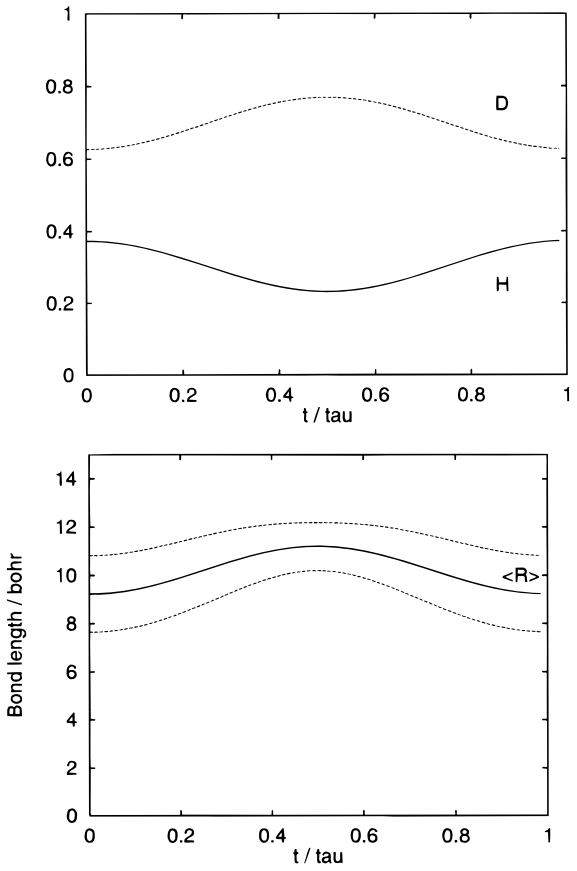

Figure 5. The electron population on the proton and on the deuteron together with the expectation value of the internuclear separation vs the time in units of the vibration period τ. Note that the electron and the nuclei move on the same time scale (i.e., breakdown of the adiabatic approximation).

the right time (without destroying the electron population on the two nuclei), we should be able to control the branching ratio between $H^+ + D$ and $H + D^+$. The electron density oscillates between 38/62% and 22/78% on H/D; however, it should be noted that, if we could make the wave packet oscillate entirely through and free from the nonadiabatic coupling, we would expect a theoretical limit of 50/50% to 0/100% for the electron density on H/D.

C. Electronic Control. Assume that we at time $t = 0$ have prepared the molecule in the coherent superposition as defined in eq 27, we now want to dissociate the molecule from this state using a femtosecond laser pulse. Further we want the time we fire the pulse to have a controlling influence on the branching ratio. Dissociation out of highly excited vibrational eigenstates using infrared picosecond laser pulses has been studied previously see, for example, ref 41.

We start out with a Gaussian pulse with a duration (full width at half-maximum, FWHM) of $\Delta t = 50$ fs and a center frequency $\omega_0 = 300$ cm^{-1}; however, these parameters we shall later vary. The peak intensity of the field is 160 MW cm^{-2} corresponding to a field strength of $E_0 = 35$ MV m^{-1}. We fire the pulse so it reaches its maximum at times $\tilde{t}$, from 0 to τ. The electric field hence takes the form:

$$E(t) = E_0 \exp[-4 \ln 2(t - \tilde{t})^2/\Delta t^2] \cos[\omega_0(t - \tilde{t})] \quad (28)$$

The calculation is again performed on two 512 point grids with a position spacing of 0.1 b, using the Lanczos[42,43] algorithm for the time evolution.

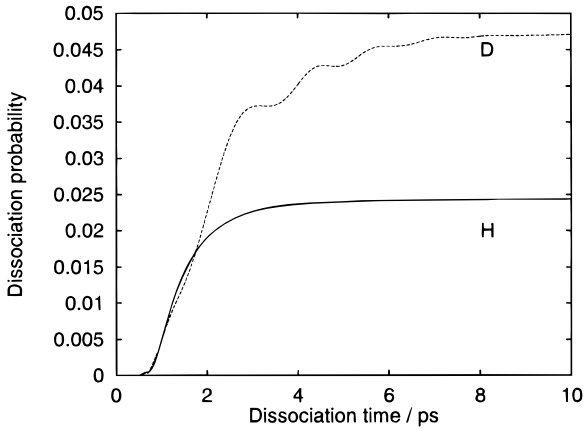

Figure 6. The amount of free deuterium and hydrogen as a function of time for $\tilde{t} = \tau/2$. The frequency of the pulse is $\omega = 300$ cm^{-1}. The dissociation takes place on picosecond scale. Note that the free deuterium arrives in chunks indicating an oscillating wave packet in the adiabatic well.

We propagate up to times $t = 10$ ps before the dissociation is over and the amount of formed hydrogen and deuterium is constant. For times that long we would in principle need an enormous grid to avoid reflection from grid boundaries; however, instead we use an absorber at the edge of the grid and add up the flux. We have tried to perform the computation with several standard absorbers (see, for example, ref 44, 45); however, they are all dependent on the wave packet being not too broad in momentum space, or otherwise they will reflect. The dissociating wave packet formed by the short laser pulse contains momenta in a large interval and hence a better absorber was needed. We used a newly derived absorber that automatically adjusts to the actual momentum. All details about this absorber can be found in ref 46.

In Figure 6, we have plotted the amount of free deuterium and hydrogen as a function of time when the laser pulse peaks at $\tilde{t} = \tau/2$. We see that the amount of free hydrogen becomes constant quite fast, whereas the amount of free deuterium arrives in chunks. This is most likely due to the adiabatic well in the electronic excited potential. It catches some of the wave packet and it leaks slowly to the electronic ground state potential as it oscillates back and forth.

The amount of free deuterium and hydrogen relative to the total yield as a function of $\tilde{t}$ is plotted in Figure 7a for a pulse width of $\Delta t = 50$ fs. We see that we get the maximum amount of deuterium when $\tilde{t} \simeq 0.6\ \tau$ and the smallest amount when $\tilde{t} \simeq 0.1\ \tau$.

If we compare the amount of deuterium from Figure 7a with the electron population on the deuteron at given times (in Figure 5) we observe a strong correlation. The maximum/minimum is not as high as in the bound molecule this we ascribe, partly, to the fact that we have a finite pulse width.

The influence of the finite pulse width becomes more evident in Figure 7b, where we have made the same calculation with $\Delta t = 100$ fs. Here the controllability is almost gone, since the pulse is averaging over many electronic and nuclear configurations. The overall yield is about the same for $\Delta t = 50$ fs and $\Delta t = 100$ fs, namely ~7%.

Finally, we have changed the frequency to $\omega_0 = 600$ cm^{-1} and we observe now that the hydrogen channel is favored. This is due to the Franck−Condon factors for the (diabatic) vibrational transitions; The Franck−Condon factor for a H-channel vibrational transition is bigger than that of a D-channel vibrational transition at this frequency. Furthermore, they are

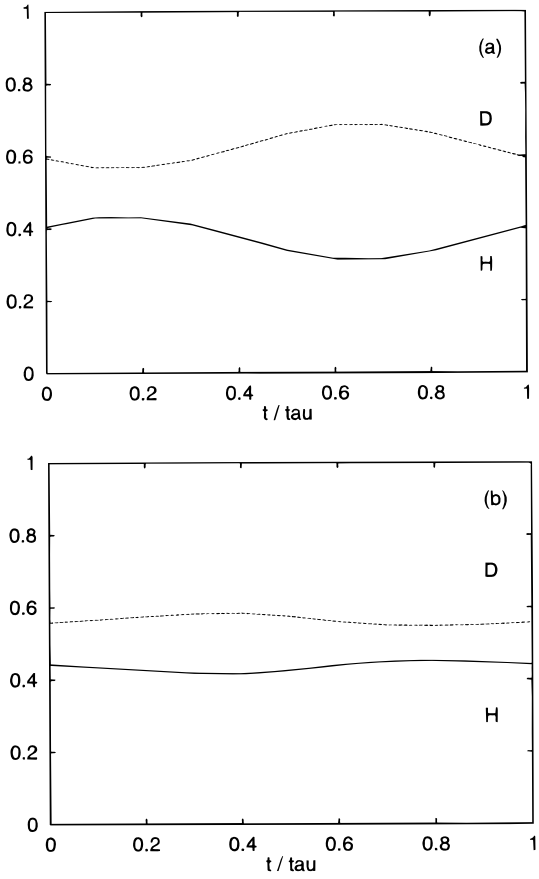

Figure 7. The percentage of free deuterium and hydrogen as a function of the time where the laser pulse is fired. The frequency of the pulse is $\omega_0 = 300$ cm^{-1} and the pulse width is (a) $\Delta t = 50$ fs and (b) $\Delta t = 100$ fs. Note that as the pulse width is increased the controllability is decreased. The overall yield is about the same for (a) and (b), namely, ~7%.

both much smaller than the Franck−Condon factors for the $\omega_0 = 300$ cm^{-1} transition resulting in a yield of only 0.5%.

IV. Conclusion

We have presented a new scheme for controlling electron transfer during the breaking of a chemical bond. The scheme goes as follows: First we create an oscillating electron in a molecule, secondly we break the bond with a short IR-laser pulse at a given time-delay corresponding to the time when the electron "sits" at the right place. The electronic motion is hereby freezed and the electron follows the fragment it was located on just before the bond-breakage.

We have presented, from first principles, the theory for HD^+ and have only introduced minor approximations, hence there is only little or no room for speculations concerning the validity of the results. We have tested the scheme on HD^+ and found it successful. We saw that we could indeed create an oscillating electron. By applying the IR-laser pulse we showed that we could break the bond and hereby freeze the electronic motion and hence control which fragment the electron should follow.

The degree of controllability is not as high as in other schemes for electronic control in HD^+.[23] The optimal control is obtained when the wave packet oscillates back and forth through the avoided crossing, such that it is completely free of this region. For HD^+ the oscillating wave packet considered in the present study is never completely free of the avoided crossing, and hence the control is not optimal. The control scheme used here might be better suited for other molecules. The implementation on NaI is in progress.[28]

Acknowledgment. The authors would like to thank Søren R. Keiding for discussions concerning electronic motion in HD^+. This work was supported by the Danish Natural Science Research Council.

References and Notes

(1) Manz, J. Molecular wavepacket dynamics: Theory for experiments 1926−1996. In *Femtochemistry and Femtobiology;* Sundström, V., Ed.; World Scientific: Singapore, 1997; in press.
(2) Gordon, R. J.; Rice S. A. *Annu. Rev. Phys. Chem.* **1997**, *48*, 601.
(3) Gaspard, P., Burghardt, I., Eds. *Adv. Chem. Phys.* **1997**, 101 (Chemical Reactions and their Control on the Femtosecond Time Scale).
(4) Grønager, M.; Henriksen, N. E. *Chem. Phys. Lett.* **1997**, *278*, 166.
(5) Tannor, D. J.; Kosloff, R.; Rice, S. A. *J. Chem. Phys.* **1986**, *85*, 5805.
(6) Rice, S. A.; Tannor, D. J.; Kosloff, R. *J. Chem. Soc., Faraday Trans. 2* **1986**, *82*, 2423.
(7) Kohler, B.; Krause, J. L.; Raksi, F.; Wilson, K. R.; Yakovlev, V. V. *Acc. Chem. Res.* **1995**, *28*, 133.
(8) Chelkowski, S.; Zuo, T.; Atabek, O.; Bandrauk, A. D., *Phys. Rev. A* **1995**, *52*, 2977.
(9) Amstrup, B.; Henriksen, N. E. *J. Chem. Phys.* **1996**, *105*, 9115.
(10) Lu, Z.-M.; Rabitz, H. *J. Phys. Chem.* **1995**, *99*, 13731.
(11) Nguyen-Dang, T. T.; Chatelas, C.; Tanguay, D. *J. Chem. Phys.* **1995**, *102*, 1528.
(12) Shen, H.; Dussault, J.-P.; Bandrauk, A. D. *Chem. Phys. Lett.* **1994**, *221*, 498.
(13) Amstrup, B.; Tóth, G. J.; Szabó, G.; Rabitz, H.; Lörincz, A. *J. Phys. Chem.* **1995**, *99*, 5206.
(14) Moss, R. E.; Jopling, D. *Chem. Phys. Lett.* **1996**, *260*, 377.
(15) Hunter, G.; Gary, B. F.; Pritchard, H. O. *J. Chem. Phys.* **1966**, *45*, 3806.
(16) Hunter, G.; Pritchard, H. O. *J. Chem. Phys.* **1967**, *46*, 2146.
(17) Hunter, G.; Pritchard, H. O. *J. Chem. Phys.* **1967**, *46*, 2153.
(18) Carrington, A.; McNab, I. R.; Montgomerie-Leach, C. A.; Kennedy, R. A. *Mol. Phys.* **1991**, *72*, 735.
(19) Wolniewicz, L.; Poll, J. D. *Can. J. Phys.* **1985**, *63*, 1201.
(20) Sheehy, B.; Walker, B.; DiMauro, L. F. *Phys. Rev. Lett.* **1995**, *74*, 4799.
(21) Ghosh, S.; Chakrabarti, M. K.; Bhattacharyya, S. S.; Saha, S. *J. Phys. B* **1995**, *28*, 1803.
(22) Ghosh, S.; Mitra, S. S.; Bhattacharyya, S. S.; Saha, S. *J. Phys. B* **1996**, *29*, 3109.
(23) Charron, E.; Giusti-Suzor, A.; Mies, F. H. *Phys. Rev. Lett.* **1995**, *75*, 2815.
(24) Brumer, P.; Shapiro, M. *Chem. Phys. Lett.* **1986**, *126*, 541.
(25) Brumer, P.; Shapiro, M. *Annu. Rev. Phys. Chem.* **1992**, *43*, 257.
(26) Brumer, P.; Shapiro, M. *Sci. Am.* **1995**, *272*, 56.
(27) Shapiro, M.; Brumer, P. *J. Chem. Soc., Faraday Trans.* **1997**, *93*, 1263.
(28) Grønager, M.; Henriksen, N. E. *J. Chem. Phys.* Submitted for publication.
(29) Born, M.; Huang, K. *Dynamical Theory of Crystal Lattices*; The Clarendon Press: Oxford, England, 1954.
(30) Abramowitz, M. A.; Stegun, I. A. *Handbook of Mathematical functions;* National Bureau of Standards: Washington, DC, 1964.
(31) Burrau, Ø. *K. Dan. Vidensk. Selsk. Skr.* **1927**, 7.
(32) Power, J. D. *Philos. Trans. R. Soc. London, Ser. B A* **1973**, *274*, 663.
(33) Teller, E., Sahlin, H. L. In *Physical Chemistry, An Advanced Treatment;* Eyring, H., Ed.; Academic Press: New York, 1970; Vol. 5, Chapter 2.
(34) Nikitin, E. E.; Umanskii, S. Y. *Theory of Slow Atomic Collisions;* Springer: Berlin, 1984; Vol. 30.
(35) Grønager, M.; Henriksen, N. E. *J. Chem. Phys.* **1996**, *104*, 3234.
(36) Kosloff, R.; Tal-Ezer, H. *Chem. Phys. Lett.* **1986**, *127*, 223.
(37) Tal-Ezer, H.; Kosloff, R. *J. Chem. Phys.* **1984**, *81*, 3967.
(38) Kosloff, R. *J. Phys. Chem.* **1988**, *92*, 2087.
(39) Fleck, J. A.; Morris, J. R.; Feit, M. D. *Appl. Phys.* **1976**, *10*, 129.
(40) Feit, M. D.; Fleck, J. A.; Steiger, A. *J. Comput. Phys.* **1982**, *47*, 412.
(41) Korolkov, M. V.; Paramonov, G. K.; Schmidt, B. *J. Chem. Phys.* **1996**, *105*, 1862.
(42) Leforestier, C.; Bisseling, R. H.; Cerjan, C.; Feit, M. D.; Friesner, R.; Guldberg, A.; Hammerich, A.; Jolicard, G.; Karrlein, W.; Meyer, H.-D.; Lipkin, N.; Roncero, O.; Kosloff, R. *J. Comput. Phys.* **1991**, *94*, 59.
(43) Park, T. J.; Light, J. C. *J. Chem. Phys.* **1986**, *85*, 5870.
(44) Vibok, A.; Balint-Kurti, G. G. *J. Phys. Chem.* **1992**, *96*, 8712.
(45) Macías, D.; Brouard, S.; Muga, J. G. *Chem. Phys. Lett.* **1994**, *228*, 672.
(46) Grønager, M. *J. Chem. Phys.* Submitted for publication.